COMPARING EFFICIENT BROADBAND BEAMFORMING ARCHITECTURES AND THEIR PERFORMANCE TRADE-OFFS

Stephan Weiss

Dept. of Electronics & Computer Science
University of Southampton
Southampton, UK
s.weiss@ecs.soton.ac.uk

Ian K. Proudler

Signal Processing Group
QinetiQ Ltd.
Greater Malvern, UK
i.proudler@signal.qinetiq.com

Abstract: In this paper, we evaluate efficient implementations of a broadband beamforming structure, that permits to project the data onto subspaces defined by the principle components of the array data. This optimum but computationally expensive approach is approximated in the frequency domain by processing in independent frequency bins. The later is computationally optimal, but suffers from spectral leakage. We show that this problem persists even if the frequency resolution is increased, and that the worst case performance depends on the available degrees for freedoms only. Further, an oversampled subband scheme is proposed, which sacrifes some computational complexity but has a considerably improved and controllable worst case performance.

1. INTRODUCTION

Broadband beamforming is a technique that uses both temporal and spatial information to separate signal components impinging on an array of M sensors from various directions of arrival (DOA). This finds applications in radar and sonar [12], or in communications to deal with multiple users operating within the same frequency band [6]. Amongst a larger number of choices for different structures [12, 6], the type of broadband beamformer considered here is a processor for the received M channel data, which can filter out signal components that occupy a certain subspace in the spatio-temporal domain by means of principle components.

To achieve high spatial and temporal resolution, large array dimensions and time windows have to be employed, thus resulting in a considerable complexity. A number of techniques have been developed to either reduce the number of degrees of freedom (DOF) and therefore the adjustable parameters in the system [13], or find numerically efficient schemes such as DFT based beamforming in the frequency domain [10, 1, 5] or subband processing [16]. The aim of this paper is to survey and compare computationally inexpensive broadband beamforming methods similarly to the ones in [1, 16] based on DFT and subband processing, for the above M-channel subspace filter.

Both frequency domain and subband methods apply a filter bank to the sensor data. The traditional choice of filter bank is a discrete Fourier transform (DFT), whereby it is hoped that in the Fourier domain interactions between different frequency bins can be neglected. This approximation as an "independent frequency bin"(IFB) processor offers computational optimality but also suffers from drawbacks due to the DFTs relatively poor frequency resolution. A second choice of filter banks are oversampled filter banks (OSFBs) that sacrifice some computational savings but avoid the drawbacks of the IFB-KLT by employing filters with a high frequency selectivity [3].

The paper is organised as follows. Sec. 2 will introduce the considered broadband beamformer or multichannel filtering structure, and the calculations of the processor matrix via principle components of the data. A frequency domain implementation analogous to e.g. [1] is performed in Sec. 3, highlighting the approximations made. Sec. 4 proposes a subband based beamformer, which in structure has similarities to the frequency domain processor. This subband processor sacrifices some computational complexity to avoid drawbacks of the frequency domain processor, which will be demonstrated when assessing the worst-case performance of these processor structures in Sec. 5.

2. OPTIMUM BROADBAND BEAMFORMING

2.1. Structure

The considered broadband beamforming structure is depicted in Fig. 1. The M channel input signal is passed into tapped delay lines (TDL), which in Fig. 1 are labelled as serial-to-parallel (s/p) conversion blocks. At the output of these TDLs, a vector $\mathbf{x}_\mathrm{I}[n]$ of spatio-temporally sampled data,

$$\begin{aligned} \mathbf{x}_\mathrm{I}^\mathrm{T}[n] &= \left[\mathbf{x}_0^\mathrm{T}[n] \;\; \mathbf{x}_1^\mathrm{T}[n] \;\cdot\; \mathbf{x}_{M-1}^\mathrm{T}[n]\right] \quad \text{with} \quad (1) \\ \mathbf{x}_m^\mathrm{T}[n] &= \left[x_m[n] \;\; x_m[n-1] \;\cdots\; x_m[n-L+1]\right] \end{aligned}$$

is passed to a processor matrix $\mathbf{T}_\mathrm{I}$. Before entering the processor matrix, the data vector $\mathbf{x}_\mathrm{I}[n]$ is generally decimated by a factor N, $1 \leq N \leq L$, where L is the length of the TDL. This decimation is part of the serial to parallel (s/p) converters in Fig. 1 which are shown in detail in Fig. 2(a). After the multiplication with $\mathbf{T}_\mathrm{I}$, the reverse process takes place, whereby the expansion by N and the multiplexing given in Fig. 2(b) define a parallel-to-serial (p/s) converter.

0–7803–7503–3/02/$17.00 ©2002 IEEE

The processor matrix $\mathbf{T}_\mathrm{I}$ is select optimally in terms of filtering based on principle components [9]. For this, first the covariance matrix of the input data vector, $\mathbf{R}_\mathrm{I} = \mathcal{E}\{\mathbf{x}_\mathrm{I}[\nu] \cdot \mathbf{x}_\mathrm{I}^\mathrm{H}[\nu]\}$ is calculated, where $\mathcal{E}\{\cdot\}$ is the expectation operator. The eigenvalue decomposition of $\mathbf{R}_\mathrm{I}$ gives

$$\mathbf{R}_\mathrm{I}\mathbf{Q} = \mathbf{Q}\mathbf{\Lambda} \quad , \tag{2}$$

where $\mathbf{Q}$ is the modal matrix and $\mathbf{\Lambda}$ a diagonal matrix containing the eigenvalues. Some of the eigenvalues and their accompanying eigenvectors in $\mathbf{Q}$ represent structured data, and by isolating selected eigenvalues, different principle components of the data can be separated. This is performed via a modified low rank approximation $\mathbf{T}_\mathrm{I}$ of the covariance matrix, which is given by

$$\mathbf{T}_\mathrm{I} = \mathbf{Q} \cdot \mathbf{\Theta}(\mathbf{\Lambda}) \cdot \mathbf{Q}^\mathrm{H} \tag{3}$$

where $\mathbf{\Theta}(\cdot)$ is a binary threshold operator.

2.2. Gain Response

To characterise the broadband beamformer described in Sec. 2.1, a gain response is calculated in the following. This response represents the absolute gain and phase that the processor imposes on a narrowband signal of normalised angular frequency Ω impinging from a direction of arrival (DOA) ϑ onto an M-element array. The sensor data can be simulated by means of a steering vector $\mathbf{s}(\Omega, \vartheta)$,

$$\mathbf{s}(\Omega, \vartheta) = \begin{bmatrix} 1 \\ e^{-j\sin(\theta)\Omega} \\ \vdots \\ e^{-j(M-1)\sin(\theta)\Omega} \end{bmatrix} \quad , \tag{4}$$

which expresses the impinging wavefront's delay to hit the different sensors of an array that is assumed to be linear and uniformly spaced. At the processor output an optimal narrowband beamformer, equivalent to a matched filter for the steering vector, is applied. The flow graph for obtaining this gain response $A(e^{j\Omega}, \vartheta)$ is given in Fig. 3. Note that for a trivial processor $\mathbf{T}_\mathrm{I} = \mathbf{I}$ forming an identity matrix, this is an optimal narrowband beamformer with $A(e^{j\Omega}, \vartheta) = \mathbf{s}^\mathrm{H}(\Omega, \vartheta) \cdot \mathbf{s}(\Omega, \vartheta) = M$.

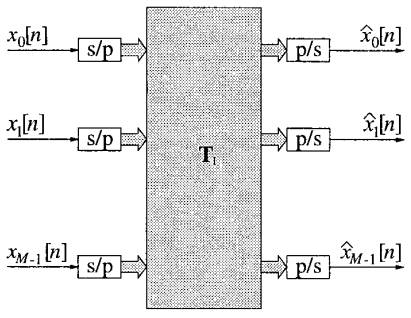

Fig. 1. Flow graph of a broadband beamforming processor for M-channel data.

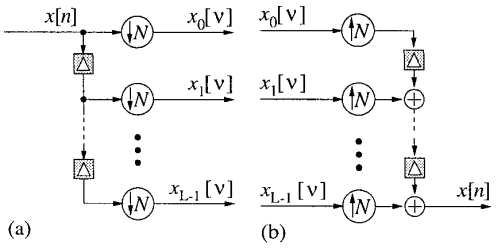

Fig. 2. (a) Demultiplexer or (s/p) block and (b) multiplexer or (p/s) block constructed from delay elements, decimators ($\downarrow N$) and expanders ($\uparrow N$).

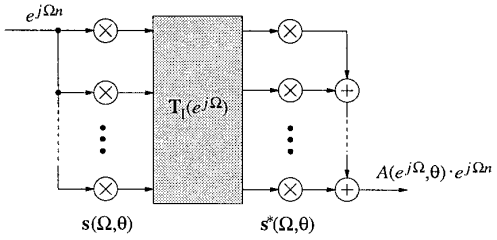

Fig. 3. Gain response $A(e^{j\Omega}, \vartheta)$ of processor; the processor block incorporates demultiplexers and multiplexers.

While generally it is not straightforward to determine $A(e^{j\Omega}, \vartheta)$ analytically, the simple case of an undecimated processor with $N = 1$ reduces to

$$A(e^{j\Omega}, \theta) = \frac{1}{L} \cdot \left(\mathbf{s}^\mathrm{H}(\Omega, \vartheta) \cdot \mathbf{F}^\mathrm{H}(\Omega) \cdot \mathbf{T}_\mathrm{I} \cdot \mathbf{F}(\Omega) \cdot \right. \\ \left. \cdot \mathbf{s}(\Omega, \vartheta)\right) \cdot e^{-j(L-1)\Omega} \tag{5}$$

where $\mathbf{F}^\mathrm{H}(\Omega)$ describes the response of the multiplexing and demultiplexing according to Fig. 2.

3. DFT-BASED BROADBAND BEAMFORMING

3.1. Structure

The application of the discrete Fourier transform (DFT) to a broadband beamforming structure is very popular as it promises computational advantages over the time domain approach [10, 1, 5]. For a frequency domain processor, the TDL in the M demultiplexing (s/p) blocks of Fig. 1 are subjected to a DFT of length L. This situation is shown in Fig. 4. The signals at the output of the DFT blocks can be denoted as vector $\mathbf{x}_{\mathrm{fd-I}}[\nu]$,

$$\mathbf{x}_{\mathrm{fd-I}}[\nu] = \mathbf{B} \cdot \mathbf{x}_\mathrm{I}[\nu] \tag{6}$$

with

$$\mathbf{B} = \mathrm{diag}\{\mathbf{T}_\mathrm{DFT}, \mathbf{T}_\mathrm{DFT}, \cdots \mathbf{T}_\mathrm{DFT}\} \quad . \tag{7}$$

The matrices $\mathbf{T}_\mathrm{DFT} \in \mathbb{C}^{L \times L}$ are DFT matrices scaled by $\sqrt{L}$ such that $\mathbf{T}_\mathrm{DFT}$ is unitary, hence $\mathbf{B}^{-1} = \mathbf{B}^\mathrm{H}$.

By a suitable permutation of the data vector, the input to the frequency domain processor can be attained as

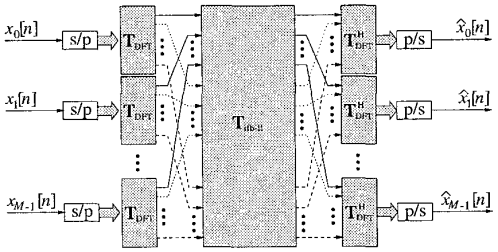

Fig. 4. Flow graph of a frequency domain processor.

indicated in Fig. 4,

$$\mathbf{x}_{\mathrm{fd-II}} = \mathbf{P} \cdot \mathbf{x}_{\mathrm{fd-I}} \quad . \tag{8}$$

where $\mathbf{P}$ performs the permutation. Using this permuted data vector, the resulting covariance matrix $\mathbf{R}_{\mathrm{fd-II}} = \mathcal{E}\{\mathbf{x}_{\mathrm{ifb-II}} \cdot \mathbf{x}^{\mathrm{H}}_{\mathrm{ifb-II}}\}$ has the structure

$$\mathbf{R}_{\mathrm{fd-II}} = \begin{bmatrix} \mathbf{R}_{0,0} & \mathbf{R}_{1,0} & \cdots & \mathbf{R}_{L-1,0} \\ \mathbf{R}_{0,1} & \mathbf{R}_{1,1} & & \mathbf{R}_{L-1,1} \\ \vdots & & \ddots & \\ \mathbf{R}_{0,L-1} & \mathbf{R}_{1,L-1} & \cdots & \mathbf{R}_{L-1,L-1} \end{bmatrix} . \tag{9}$$

In (9), $\mathbf{R}_{i,j}$ is an $M \times M$ correlation matrix between frequency bins i and j of different sensor signals .

The covariance matrix $\mathbf{R}_{\mathrm{fd-II}}$ can be related to the covariance matrix in the time-domain case by (6) as

$$\mathbf{R}_{\mathrm{fd-II}} = \mathbf{P} \cdot \mathbf{B} \cdot \mathbf{R}_{\mathrm{I}} \cdot \mathbf{B}^{\mathrm{H}} \cdot \mathbf{P}^{\mathrm{H}} \quad . \tag{10}$$

Due to the unitarity of $\mathbf{P} \cdot \mathbf{B}$, $\mathbf{R}_{\mathrm{fd-II}}$ and $\mathbf{R}_{\mathrm{I}}$ have identical eigenvalues [7]. If the eigenvalues of $\mathbf{R}_{\mathrm{fd-II}}$ are subjected to the same binary thresholding as in the time domain processor matrix in (3), then the frequency domain processor with matrix $\mathbf{T}_{\mathrm{fd-II}} = \mathbf{P}\mathbf{B}\mathbf{T}_{\mathrm{I}}\mathbf{B}^{\mathrm{H}}\mathbf{P}^{\mathrm{H}}$ differs structurally from the time domain processor in Sec. 2, but can implement the identical functionality.

3.2. Approximations

In general, frequency domain methods neglect any interaction between adjacent frequency bins. Therefore in DFT-based beamforming, a computational advantage arises as within each frequency bin only a narrowband beamformer is operated independently of the ones operated in other frequency bins [1]. For the covariance matrix of the resulting processor, the restriction to infra-bin processing results in a modification of the matrix structure in (9),

$$\mathbf{R}_{\mathrm{ifb}} = \begin{bmatrix} \mathbf{R}_{0,0} & \mathbf{O}_L & \cdots & \mathbf{O}_L \\ \mathbf{O}_L & \mathbf{R}_{1,1} & & \mathbf{O}_L \\ \vdots & & \ddots & \vdots \\ \mathbf{O}_L & \mathbf{O}_L & \cdots & \mathbf{R}_{L-1,L-1} \end{bmatrix} , \tag{11}$$

i.e. correlations between different bins $i \neq j$ are set to zero.

The eigenvalue decomposition of $\mathbf{R}_{\mathrm{ifb}}$ can be reduced to solving eigenvalue problems for the L sub-matrices $\mathbf{R}_{i,i}$ independently, with the result that an identical block-diagonal structure is achieved for the processor matrix $\mathbf{T}_{\mathrm{ifb}}$ containing $L \times L$ sub-matrices. The subscript used in the above quantities refers to the processing in independent frequency bins (IFB).

Although the approximations in (11) make the IFB-processor optimal in the sense of computational complexity, spectral leakage will create a problem whenever input data does not exactly lie on a frequency bin. The effect will be highlighted in Sec. 5.

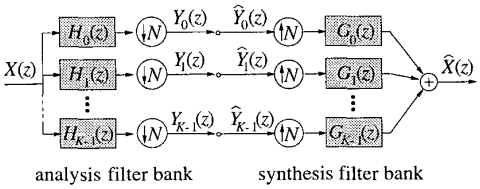

Fig. 5. K channel analysis and synthesis filter bank with decimation and expansion by $N \leq K$.

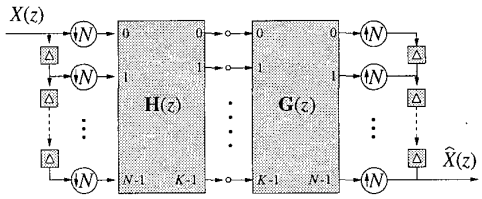

Fig. 6. Equivalent filter bank representation to Fig. 5 with polyphase analysis and synthesis matrices, $\mathbf{H}(z)$ and $\mathbf{G}(z)$.

4. SUBBAND-BASED BROADBAND BEAMFORMING

Interpreting the L-point DFT in Sec. 3 as an L channel filter bank of poor selectivity, spectral leakage can be suppressed by employing filters with better frequency domain properties. This leads to the subband-based structure discussed below.

4.1. Oversampled Frequency Bands

A general K-channel filter bank with analysis and synthesis of a fullband signals is shown in Fig. 5. In the analysis bank, after filtering with bandpass filters $H_k(z)$ the resulting subband signals have reduced bandwidth and can therefore be decimated by $N < K$. If the $H_k(z)$ are selective enough, only a low aliasing level is incurred in the decimation process. A fullband signal can be reconstructed by expanding the subbands signals by N, and combining them after interpolation filtering with $G_k(z)$, as shown in Fig. 5. An equivalent filter bank representation by polyphase analysis and synthesis matrices $\mathbf{H}(z)$ and $\mathbf{G}(z)$ is shown in Fig. 6, which offers advantages for circuit analysis and numerically efficient implementation [2, 11, 3, 14].

Perfect reconstruction $\hat{X}(z) = z^{-\Delta}X(z)$ can be conveniently established if the polyphase analysis matrix is paraunitary, i.e. $\tilde{\mathbf{H}}(z)\cdot\mathbf{H}(z) = \mathbf{I}$ where $\tilde{\mathbf{H}}(z) = \mathbf{H}^{\mathrm{H}}(z^{-1})$. In this case a perfectly reconstructing synthesis filter bank is given by setting $\mathbf{G}(z) = \tilde{\mathbf{H}}(z)$, as can be easily verified from Fig. 6. In practice, the perfect reconstruction condition can be relaxed by allowing small errors in the reconstruction. This error, together with the level of aliasing, can be controlled by the filter bank design [8].

By oversampling $N < K$ aliasing in the subbands is suppressed, at the expense of introducing redundancy into the subband domain. This however is advantageous in many applications, as the redundancy lies in the overlapping region of the analysis filters $H_k(z)$. This fact enables to treat different subbands independently, and decouples the problem of processing between adjacent subbands as found in the critically sampled case $N = K$ [4] or the DFT-structure in Sec. 3.

4.2. Beamforming Structure

Substituting the filter bank blocks in Fig. 6 into the DFT-based broadband beamforming processor of Sec. 3, the subband structure in Fig. 7 emerges. All M sensor signals are decomposed by analysis filter banks, while the dual operation is performed at the processor output. The signal vector $\mathbf{x}_{\mathrm{sub}}[\nu]$ fed into the processor matrix is given by

$$\begin{aligned} \mathbf{x}_{\mathrm{sub}}^{\mathrm{T}}[\nu] &= [\mathbf{x}_0[\nu]\,\mathbf{x}_1[\nu]\,\cdots\,\mathbf{x}_{K-1}[\nu]] \quad \text{with} \quad (12)\\ \mathbf{x}_k^{\mathrm{T}}[\nu] &= [\mathbf{x}_{0,k}[\nu]\,\mathbf{x}_{1,k}[\nu]\,\cdots\,\mathbf{x}_{M-1,k}[\nu]]\ ,\\ \mathbf{x}_{m,k}^{\mathrm{T}}[\nu] &= [x_{m,k}[\nu]\,x_{m,k}[\nu-1]\,\cdots\,x_{m,k}[\nu-L_s+1]]\,. \end{aligned}$$

Since the subband signals are relatively broadband due to decimation, TDLs of length L_s have been applied to each subband. The value for L_s can be selected considerably shorter than L in the fullband case, but for identical number of degrees of freedom (DOF) compared to the standard broadband processor in Sec. 2, $L_s = L/K$ can be set.

The covariance matrix of the data vector $\mathbf{x}_{\mathrm{sub}}[\nu]$ in (12), $\mathbf{R}_{\mathrm{sub}} = \mathcal{E}\{\mathbf{x}_{\mathrm{sub}}\cdot\mathbf{x}_{\mathrm{sub}}^{\mathrm{H}}\} \in \mathbb{Z}^{MKL_s\times MKL_s}$, takes the structure

$$\mathbf{R}_{\mathrm{sub}} = \begin{bmatrix} \mathbf{R}_{0,0} & \mathbf{R}_{1,0} & \cdots & \mathbf{R}_{K-1,0} \\ \mathbf{R}_{0,1} & \mathbf{R}_{1,1} & & \mathbf{R}_{K-1,1} \\ \vdots & & \ddots & \\ \mathbf{R}_{0,K-1} & \mathbf{R}_{1,K-1} & \cdots & \mathbf{R}_{K-1,K-1} \end{bmatrix}. \quad (13)$$

The sub-matrices $\mathbf{R}_{i,j}$, $i,j \in \{0; K-1\}$ are spatio-temporal covariance matrices between the ith and jth subband. If the filter banks have a high frequency selectivity and the resulting subbands only overlap with one adjacent band [4], then $\mathbf{R}_{i,j} \approx \mathbf{0}_{ML_s}\forall|i-j|>1$ except for the corner matrices $\mathbf{R}_{0,K-1}$ and $\mathbf{R}_{K-1,0}$.

4.3. Approximation

The computational efficiency of the proposed subband-based processor is not only due to neglecting the spatio-temporal sub-matrices $\mathbf{R}_{i,j} \approx \mathbf{0}_{ML}\forall|i-j|>1$, but also all sub-matrices off the block diagonal of $\mathbf{R}_{\mathrm{sub}}$. In retaining only the matrices $\mathbf{R}_{k,k}$, for $k = 0(1)K-1$, an error would be incurred if the filter banks were critically decimated. This error-free approximation of omitting non-zero correlation terms has been similarly noted for subband adaptive filtering where the redundancy in employing oversampled filter banks (OSFB) relieves from the use of adaptive filters between adjacent subbands [4, 14, 15].

The subband-based processor matrix is built from the reduced subband covariance matrix

$$\tilde{\mathbf{R}}_{\mathrm{sub}} = \mathrm{diag}\{\mathbf{R}_{0,0},\ \mathbf{R}_{1,1},\ \cdots\ \mathbf{R}_{K-1,K-1}\} \quad (14)$$

via an eigenvalue decomposition (2) and the binary thresholding of the eigenvalues in (3), yielding the matrix $\mathbf{T}_{\mathrm{sub}}$ employed in Fig. 7. Since the eigenvalue decomposition of $\tilde{\mathbf{R}}_{\mathrm{sub}}$ comes down to K eigenvalue decompositions of $\mathbf{R}_{k,k}$, the processor matrix $\mathbf{T}_{\mathrm{sub}}$

$$\mathbf{T}_{\mathrm{sub}} = \mathrm{diag}\{\mathbf{T}_{\mathrm{sub},0},\ \mathbf{T}_{\mathrm{sub},1},\ \cdots\ \mathbf{T}_{\mathrm{sub},K-1}\} \quad (15)$$

has a block diagonal structure.

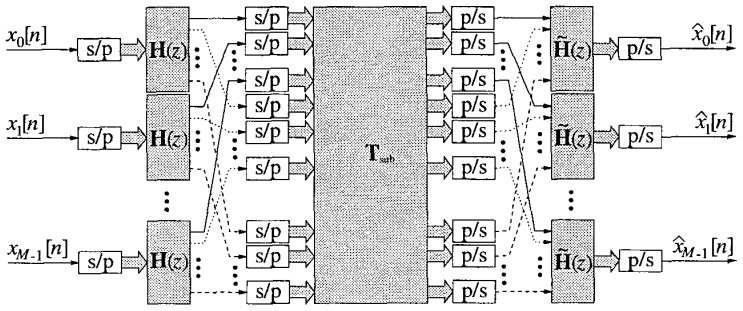

Fig. 7. Flow graph of a subband-based broadband beamforming processor.

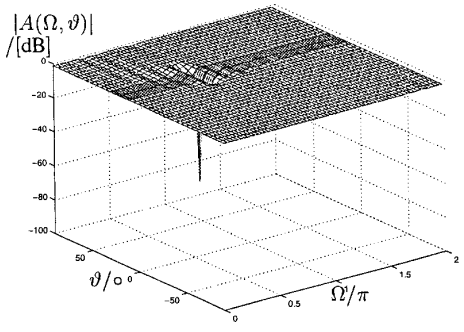

Fig. 8. Gain response of an inverse time domain processor adjusted to suppress a complex harmonic.

5. PERFORMANCE

To assess the performance of the three discussed broadband beamforming structures, Sec. 5.1 introduces the test modalities, while the results are discussed in Sec. 5.2.

5.1. Simulation Scenario

The data of the simulation is produced by a complex harmonic of frequency Ω impinging from a DOA of $\vartheta = 30°$ onto an $M = 8$ element array. For this data, covariance matrices are calculated for all cases. A broadband beamforming processor matrix is calculated for each structure such that the complex harmonic should be suppressed as best as possible. This is achieved by setting the corresponding eigenvalue in (3) to zero and all other eigenvalues to unity.

In the absence of noise, for the ideal time domain processor a single DOF would suffice to perfectly null out the signal of interest. An example for the resulting gain response in this case is given in Fig. 8. Hence the focus is on how IFB- and subband-processors can cope with this situation. The IFB-processor is characterised by an $L = 16$ point DFT, with a characteristic shown in Fig. 9. The filter bank employed for the subband-processor has $K = 8$ channels decimated by $N = 7$ depicted in Fig. 10. Subsequently, to achieve the same number of DOFs as the IFB-processor, $L_s = 2$.

5.2. Results and Discussion

The result of modifying the frequency between the 2nd and 4th bin frequency of the employed DFT is shown in Fig. 11. If the frequency of the complex harmonic coincides with a bin frequency at $\Omega = \{\frac{1}{8}\pi, \frac{1}{4}\pi \frac{3}{8}\pi\}$ infinite attenuation is achieved. For values in between the bin frequencies, spectral leakage occurs and neighbouring frequency bins are required to be adjusted in order to achieve a reasonable attenuation.

With a single eigenvalue considered, and hence a single DOF, only the closest frequency bin is active and can contribute toward attenuating the signal. Similarly, for two considered eigenvalues, the two adjacent bins contribute and improve performance over the single DOF

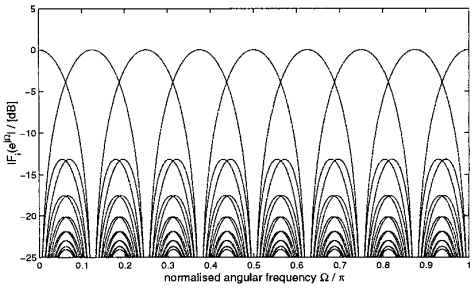

Fig. 9. Filter bank characteristic of a 16-point DFT.

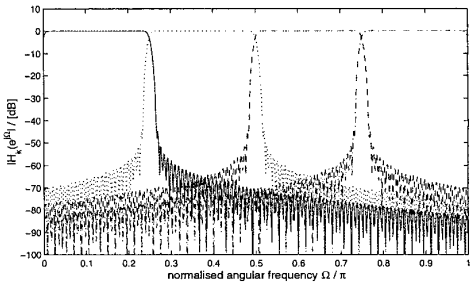

Fig. 10. Filter bank characteristic of a subband system with $K = 8$ channels decimated by $N = 7$.

case. It becomes clear that for optimal suppression, in the worst case all frequency bins need to be active, i.e. all $L = 16$ temporal DOFs will be taken up to suppress a single complex harmonic, as opposed to a single DOF required by the time domain processor. Vice versa, if only one (two) DOF is available in the IFB processor to suppress a single complex harmonic, then in the worst case the achieved attenuation will only be 5 dB (14.5 dB). This worst case occurs for complex harmonics whose frequency lies exactly between DFT bin frequencies.

Increasing the length L in the DFT of the IFB processor might be believed to influence the precision and therefore the worst-case scenario. However, independent of the number of frequency bins, the chance for signal

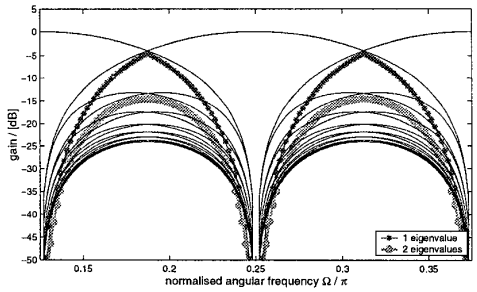

Fig. 11. Gain of the inverse IFB-KLT processor at a variable specified frequency Ω and fixed DOA considering one or two eigenvalues.

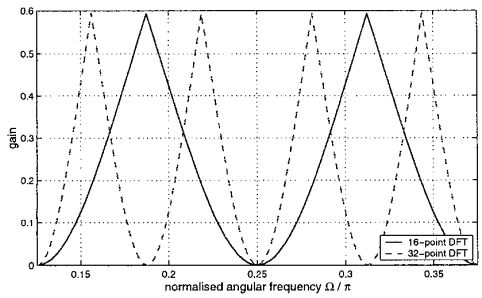

Fig. 12. Gain value as in Fig. 11, but for both $L = 16$ and $L = 32$.

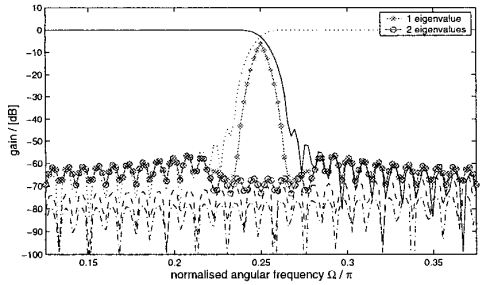

Fig. 13. Gain of the inverse subband-KLT processor considering one or two eigenvalues, adjusted to suppress a complex harmonic at a frequency varying over the 0th and 1st subband; the filter bank characteristic is underlaid.

components to fall in between bins does not decrease. In fact, doubling the frequency bins $L = 32$ and using a single eigenvalue, it is obvious from Fig. 12 that there is no change in the worst case attenuation over the earlier case $L = 16$. There is no performance gain achieved when increasing the DFT length, unless the signal's frequency is known a priori.

Similarly, the subband-processor is tested by varying the frequency of a complex harmonic across a subband edge. The results in Fig. 13 indicate that for nulling a complex harmonic outside the overlap region between two subbands, considering a single eigenvalue in the construction of the inverse processor matrix is sufficient. The achievable gain is limited by the stopband attenuation of the filter bank, as clearly the performance curve in Fig. 13 follows the stopband ripple of the filter bank. In the overlap region, the eigenvalue has to be assigned to one subband, while the remaining subband will still pass the signal and therefore deteriorate the system performance. However, if two eigenvalues are permitted, then the processor can be correctly adjusted using one DOF in each subband.

Therefore, the Subband-KLT very well approximates the ability of the TDL-KLT to express a signal subspace using up as few DOFs as possible. For a complex harmonic, in most cases one DOF will be sufficient, and a maximum of two DOFs be required in the worst case. If the frequency bands are reasonably selective and the overlap regions narrow, then in only few cases a signal component will cover the subband edges and require the latter consideration of eigenvalues in both adjacent subbands. The worst case attenuation performance, here -55 dB for the two eigenvalue case, depends only on the filter bank's stopband attenuation and is independent of the number of employed frequency bands. If two eigenvalues are permitted to suppress a complex harmonic, the worst case attenuation can, different from the IFB-KLT, always be controlled by appropriate filter design [8].

6. CONCLUSIONS

This paper has discussed an M channel filter structure for broadband beamforming, which can project onto or away from signal subspaces by means of principle components of the data. A DFT-based structure commonly employed in broadband beamforming has been used to find a numerically efficient implementation of this beamformer in form of an IFB processor. Further, a subband based processor has been proposed to bypass some drawbacks of this IFB processor.

By analysing the worst case performance, it has been shown that the performance of the IFB-beamformer is independent of the number of frequency bins but always limited by the number of DOFs that can be dedicated to process a specific subspace. In the subband case, the performance is limited by the stopband attenuation of the employed filter banks, which however can be controlled by design to be just good or poor enough for the specific application.

In general, the subband-processor forms a link between the costly time-domain processor and the poorly performing IFB approach. In the extreme case, the number of subbands in the subband processor can be lowered to $K = 1$ resulting in the time domain methods. Similarly, by setting $K = L$ and making the analysis filters poorly frequency selective, the IFB processor results. Hence, the proposed subband processor permits to tradeoff between the disadvantages of costly time domain and poorly performing IFB beamformers.

REFERENCES

[1] R. T. Compton. "The Bandwidth Performance of a Two-Element Adaptive Array with Tapped Delay-Line Processing". *IEEE Transactions on Antennas and Propagation*, Vol.36(No.1):pp.4–14, January 1988.

[2] R. E. Crochiere and L. R. Rabiner. *Multirate Digital Signal Processing*. Prentice Hall, Englewood Cliffs, NJ, 1983.

[3] Z. Cvetković and M. Vetterli. Oversampled Filter Banks. *IEEE Transactions on Signal Processing*, 46(5):1245–1255, May 1998.

[4] A. Gilloire and M. Vetterli. Adaptive Filtering in Subbands with Critical Sampling: Analysis, Experiments and Applications to Acoustic Echo Cancelation. *IEEE Transactions on Signal Processing*, SP-40(8):1862–1875, August 1992.

[5] L. C. Godara. Application of the Fast Fourier Transform to Broadband Beamforming. *Journal of the Acoustic Society of America*, 98(1):230–240, July 1995.

[6] L. C. Godara. Application of Antenna Arrays to Mobile Communications, Part II: Beam-Forming and Direction-of-Arrival Estimation. *Proceedings of the IEEE*, 85(8):1195–1245, August 1997.

[7] G. H. Golub and C. F. Van Loan. *Matrix Computations*. John Hopkins University Press, Baltimore, Maryland, 3rd edition, 1996.

[8] M. Harteneck, S. Weiss, and R. W. Stewart. Design of Near Perfect Reconstruction Oversampled Filter Banks for Subband Adaptive Filters. *IEEE Transactions on Circuits & Systems II*, 46(8):1081–1086, August 1999.

[9] T. K. Moon and W. C. Stirling. *Mathematical Methods and Algorithms*. Prentice H ll, Upper Saddle River, NJ, 1999.

[10] D. Nunn. Suboptimal Frequency-Domain Adaptive Antenna Processing Algorithm for Broad-Band Environments. *IEE Proc. F: Radar and Signal Processing*, 134(4):341–351, July 1987.

[11] P. P. Vaidyanathan. *Multirate Systems and Filter Banks*. Prentice Hall, Englewood Cliffs, 1993.

[12] B. D. Van Veen and K. M. Buckley. Beamforming: A Versatile Approach to Spatial Filtering. *IEEE Acoustics, Speech, and Signal Processing Magazine*, 5(2):4–24, April 1988.

[13] B. D. Van Veen and R. A. Roberts. Partially Adaptive Beamforming Design via Output Power Minimization. *IEEE Transactions on Acoustics, Speech, and Signal Processing*, 35:1524–1532, 1987.

[14] S. Weiss. *On Adaptive Filtering in Oversampled Subbands*. PhD thesis, Signal Processing Division, University of Strathclyde, Glasgow, May 1998.

[15] S. Weiss, A. Stenger, R. W. Stewart, and R. Rabenstein. Steady-State Performance Limitations of Subband Adaptive Filters. *IEEE Transactions on Signal Processing*, 49(9):1982–1991, September 2001.

[16] S. Weiss, R. W. Stewart, M. Schabert, I. K. Proudler, and M. W. Hoffman. An Efficient Scheme for Broadband Adaptive Beamforming. In *Asilomar Conference on Signals, Systems, and Computers*, volume I, pages 496–500, Monterey, CA, November 1999.